Journal of Structural Geology, Vol. 10, No. 6, pp. 541 to 553, 1988
Printed in Great Britain

0191-8141/88 $03.00 + 0.00

Theory of chocolate tablet boudinage

S. K. GHOSH

Department of Geological Sciences, Jadavpur University, Calcutta—700 032, India

(*Received* 5 *October* 1987; *accepted in revised form* 20 *April* 1988)

Abstract—Two-dimensional boudinage in a flattening type of bulk deformation, with equal layer-parallel extensions in all directions, leads to the development of roundish or polygonal outlines of boudins in plan-view. As combined experimental and theoretical studies show, chocolate tablet boudinage with two sets of mutually perpendicular boudin axes may form in different ways. (1) Unequal layer-parallel extension in the matrix results in one set of extension fractures forming perpendicular to the greatest principal stress in the matrix. Once these long narrow boudins are formed, the greatest principal stress in the brittle layer becomes approximately parallel to the long axis of the boudin. As a result a second set of fractures forms normal to the first set. (2) In lineated rocks the anisotropy of tensile strength leads to the sequential formation of two sets of extension fractures, parallel and perpendicular to the lineation. Depending on the orientation of the lineation the boudin axes may or may not be parallel to the principal stresses in the matrix. (3) Boudins with rectangular plan-view may also form when two successive events of unidirectional boudinage are superposed on one another. Irrespective of the direction of principal extensional strain rate in the matrix, the second generation extension fractures are likely to form approximately perpendicular to the first generation boudin axes.

INTRODUCTION

SINCE the term chocolate tablet boudinage was used by Wegmann (1932) to describe two-dimensional boudinage in competent layers, similar structures have been described by a number of authors from several areas (e.g. Ramberg 1955, Coe 1959, Fyson 1962, Ramsay 1967, Schwerdtner & Clark 1967, Casey *et al.* 1983, Ghosh & Sengupta 1987). Both Coe and Fyson recorded two sets of boudin neck lines at right angles to each other. There is a general agreement that chocolate tablet structures develop in a flattening type of bulk deformation.

In the course of structural studies in Indian Precambrian terrains, the present author has encountered chocolate tablet boudinage in several areas. The plan-view of the structures is particularly well-exposed in the thin cherty layers of the iron formation of the Ramagiri schist belt, Andhra Pradesh, in the Chotanagpur Gneissic Complex near Jasidih, Bihar, in the mylonites of the Singhbhum Shear Zone, Bihar (Ghosh & Sengupta 1987) and in the Aravalli metasediments of the Udaipur district, Rajasthan (Naha & Halyburton 1977). Although the plan-view in some cases shows a lack of linear orientation of the extension fractures separating the boudins, the majority of the chocolate tablet structures show two sets of boudin axes or neck lines at a high angle to each other; in the different exposures this angle ranges between 70 and 90° and is close to 90° in many cases. Except in the Ramagiri area, where a late lineation is superimposed on the boudins, their axes are parallel and perpendicular to a prominent mineral lineation. In certain places, especially in the Jasidih area where boudinage and pinch-and-swell structures are closely associated, chocolate tablet structures developed by pinching-and-swelling in one direction and by boudinage in the other, with boudin axes parallel to the lineation and neck lines of pinch-and-swells roughly transverse to it. If both these structures developed during a progressive deformation, this would imply that the ductility of the rocks was greater in a direction parallel to the lineation than perpendicular to it.

It is noteworthy that, according to Naha & Halyburton (1977), some of the chocolate tablet structures in the Aravalli metapelites were formed by superposed deformations with the development of a second generation of extension fractures sub-normal to the first generation boudin axes.

Several authors have dealt with the problem of initiation of chocolate tablet boudinage (e.g. Wegmann 1932, Ramberg 1955, Ramsay 1967, Schwerdtner & Clark 1967, Sanderson 1974, Casey *et al.* 1983). The present investigation is essentially concerned with the following problems which emerged from the field observations.

(1) Why should two prominent directions of boudin axes prevail in a large number of chocolate tablet structures? Ramberg (1955) has considered the case of boudinage under an axially symmetric bulk flow of the matrix. His theory predicts that, when the far-field layer-parallel strain rates in the matrix are equal in all directions the resulting extension fractures in the brittle layer will not have any preferred orientation. On the other hand, as Ramsay (1967, p. 112) and Sanderson (1974, p. 658) have pointed out, a flattening type of bulk deformation cannot cause the *simultaneous* development of two orthogonal sets of fractures in a competent bed; if the layer-parallel matrix strain rates are unequal, it seems reasonable to expect that only one set of fractures will form perpendicular to the direction of maximum rate of extension.

(2) If there is a contrast in ductility in different directions in a lineated rock, how will this mechanical anisotropy affect the development of boudinage?

(3) The existing theories of unidirectional boudinage and of boudinage in axially symmetric deformation deal with plates and fibres symmetrically oriented with respect to the principal stresses in the matrix (Ramberg 1955, Lloyd & Ferguson 1981, Lloyd *et al.* 1982). These theories indicate that the viscous drag or shear strain of the matrix at the contact of the embedded elastic plate exerts an external force on the plate. The tensile stress on the plate depends not only on the magnitude of this force at a point but also on the length of the plate in the direction in which the force acts. In cases of superposed deformation an early generation of boudin axes may not be parallel to the principal strain rate of the matrix in the second deformation. To what extent will the tensile stress in the competent unit in the second deformation depend on the shape and orientation of the first generation boudins?

The present paper describes analogue experiments and theoretical studies which address these problems. In designing the experiments the embedding of a brittle plate in a viscous medium was avoided, mainly for two reasons. (1) In the embedded layer the initiation of fractures and the progressive evolution of boudinage cannot be observed. (2) For the viscous drag to be effective on the plate, the matrix must stick firmly to the plate. Therefore, a surface of the fractured embedded plate cannot be uncovered without disturbing the pattern of fractures. Thus the experiments were designed in such a way that boudinage in a thin plate could take place by the action of the viscous force acting from below while the upper surface of the model remained free.

EXPERIMENTAL PROCEDURE

General

The experiments described in this section involve the placing of a thin plate of partially dried plaster of Paris on the horizontal surface of a slab of pitch and allowing the pitch to flow, either by its own weight or by a uniaxial extension. In the different experiments the flow of the pitch was of three types: (1) axially symmetric, with equal rates of extension in all radial directions in the horizontal plane, (2) unequal rates of extension in two horizontal directions, with $\dot{\varepsilon}_x > \dot{\varepsilon}_y > 0$ and (3) uniaxial extension in one horizontal direction.

Types of flow in the matrix

To achieve an axially symmetric flow, a circular cylinder of pitch was prepared (Fig. 1) with a vertical axis of about 80 mm and a diameter of about 170 mm. It was placed on a glass plate, the surface of which was wetted with soap solution to avoid sticking of the pitch to the glass. The side of the cylinder was wrapped by a 15 mm thick wall of modelling clay with an inner lining of polythene. The pitch slab with its side wall was allowed to stand on the glass plate for some time till small irregularities on the upper horizontal surface were smoothened out. After placing a brittle plate of plaster of Paris on its upper surface, the pitch was allowed to flow by taking away the side wall of modelling clay and polythene, the latter preventing the sticking of pitch to the modelling clay. It may be noted that a polythene sheet sticks fast to pitch but can be easily removed without causing permanent deformation provided it is taken off by sharp tugs and not by a slow pull.

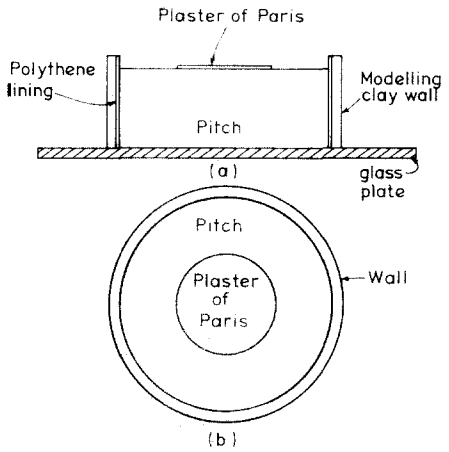

Fig. 1. (a) Vertical section and (b) plan-view showing the elements of a pitch model for axially symmetric flow.

After the flow of the pitch has started, the experiment lasts a few minutes only and successive stages of deformation are photographed. During the experiment the upper surface of the cylinder remains essentially horizontal and circular in outline although the diameter of the circle progressively increases.

In another group of experiments a thin brittle plate was subjected to unequal extensions in two mutually perpendicular directions. The pitch cylinder for this purpose was built up in two parts—a thick lower slab and a thin upper disk. A circular aluminium plate of 1.5 mm thickness and 100 mm diameter was cut into parallel strips each of 12.5 mm width. The reassembled plate (Fig. 2) was placed at the centre of the upper surface of the lower cyclinder of pitch. The thin disk of pitch and the plaster of Paris plate were placed on top of it and the assembled pitch cylinder then allowed to deform as before. A circular marker line on the pitch surface around the brittle plate was deformed into an ellipse with both diameters progressively increasing in length but at different rates (Fig. 2). A small variation in the ratio of the bulk strain rates $\dot{\varepsilon}_x$ and $\dot{\varepsilon}_y$ in the two directions could be made by adjusting the thickness of the upper disk. If the metal strips were embedded too deeply, the effect of their displacements was negligible on the upper surface of the pitch. On the other hand, if the strips were embedded too close to the surface they produced extension in only one direction on the upper surface, with $\dot{\varepsilon}_y \approx 0$. A biaxial extension with perceptible difference between the two strain rates was

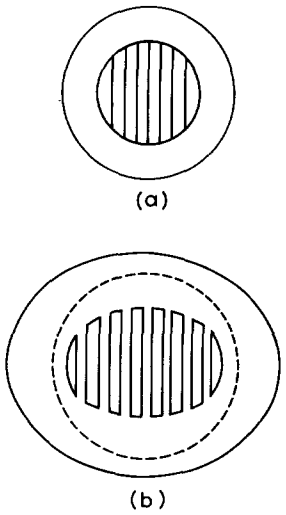

Fig. 2. Method of inducing unequal flow near the surface of a pitch slab. (a) The inner circle is a circular metal plate cut into eight parallel strips. The metal plate lies embedded about 1–1.5 cm below the top surface of the pitch cylinder. The outer circle represents a marker circle on the top surface of pitch. (b) Displacement of the embedded metal strips and deformation of marker circle on the upper surface during the flowing out of the pitch.

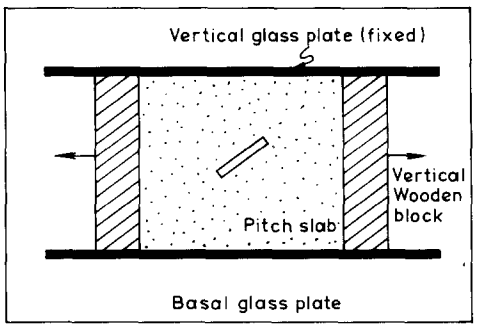

Fig. 3. Arrangement for inducing uniaxial extension in pitch slab (stippled). The basal glass plate and the inner walls of vertical glass plates are moistened with soap water. The oblique strip at the centre is a thin horizontal plate of plaster of Paris resting on the horizontal surface of pitch slab. The vertical glass plates are held in position while the two wooden blocks are slowly pulled apart.

obtained when the thickness of the upper disk ranged between 10 and 15 mm. With such thicknesses of the upper disk, the ratio $\dot{\varepsilon}_x/\dot{\varepsilon}_y$ within the first few minutes ranged between 1.2 and 1.4.

For the third group of experiments a rectangular slab of pitch was placed on the wet surface of a glass plate. The long vertical edges were confined between two fixed vertical glass plates with wet inner faces. The short vertical edges were stuck fast to two wooden blocks (Fig. 3). For uniaxial tension, the wooden blocks were slowly pulled apart. On its upper surface the length of the pitch slab progressively increased, while the width remained essentially the same.

Placing of brittle plate

The brittle plates were of three types (a) circular, (b) rectangular with a large length/width ratio and (c) circular with a lineation. For the first two types the upper surface of pitch was covered with a thin polythene sheet from which a circular or rectangular hole had been cut out. A thin slurry of plaster of Paris was sprayed on the exposed surface of pitch. The consistency of the slurry was such that it was thin enough to be sprayed smoothly (Fig. 4a). The plaster of Paris plates were about 1 mm or less in thickness. After the plaster of Paris had partially dried, the polythene sheet was taken off. The experiment was started, i.e. the confining walls removed, only after the plaster of Paris had dried to a correct consistency. A long period of drying makes the plate so strong that it does not undergo fracture or permanent deformation under the action of the viscous drag, whereas with a short period of drying it deforms homogeneously, without the development of fracture. In most cases a period of 5–8 min of drying gave good results.

In one type of model, the exposed circular surface of pitch was coated by applying the plaster of Paris with a brush. The parallel brush marks gave a lineated appearance to the plaster of Paris sheet (Fig. 4e). Because of the brush marks or fine grooves-and-ridges, the sheet of plaster of Paris became mechanically anisotropic; its tensile strength parallel to the 'lineation' was greater than in a perpendicular direction. This structural anisotropy could be produced only because the sheet of plaster of Paris was thin. The brush marks are in too fine a scale to cause significant strength variation in a thick plate.

EXPERIMENTAL RESULTS

Experiments under axially symmetrical flow

With axially symmetrical flow of the pitch slab, an overlying circular plate of plaster of Paris (Fig. 4a) developed a network of fine cracks within a few seconds. As expected, there was no preferred orientation of the fractures; the boudins in plan view were equant and somewhat roundish or polygonal (Fig. 4b). However, in a narrow, peripheral zone of the plate there were only radial fractures. The same type of boudins were also obtained when the brittle plate was square (Fig. 4c). This pattern is consistent with the radial and tangential stress distributions obtained theoretically by Ramberg (1955, equations 32 and 33). Ramberg's equations show that the radial stress σ_{rr} vanishes at the periphery, but the tangential stress $\sigma_{\theta\theta}$ does not vanish. Hence, only radial fractures are expected to form near the periphery.

Under similar axially symmetrical flow of the matrix, an entirely different pattern of extension fractures was produced when the overlying brittle plate was in the form of a long narrow rectangular strip. In this case only one set of parallel extension fractures formed, essentially perpendicular to the long axis of the plate (Fig. 4d). The modes of development of the fractures were of two types. A single mid-point fracture developed if the plate had not undergone any perceptible pre-fracture permanent deformation. Each of the fragments was then sub-

divided into boudins by a sequential development of fractures (Ramberg 1955, Lloyd *et al.* 1982). On the other hand if the pre-fracture plastic deformation was large, the fractures developed essentially at the same time at more than one point (Fig. 4d).

In another series of experiments a lineated circular sheet was subjected to an axially symmetrical flow of the matrix. The lineated sheet (Fig. 4e) produced a set of fractures parallel to the lineation almost simultaneously. With continued flow in the matrix the parallel strips or boudins were separated from each other, while each of the strips were further broken up into rectangular fragments by the development of one or more fractures perpendicular to the length of the strip (Fig. 4f). The chocolate tablet boudins in these experiments were thus produced by sequential development of two mutually perpendicular sets of fractures. The orientation of the first set of fractures was controlled by the lineation while the orientation of the second set was determined by the orientation of the long axis of the first set of boudins. The time interval between the development of the two sets of fractures varied in the different experiments, presumably due to variation in stength of the plaster of Paris plate.

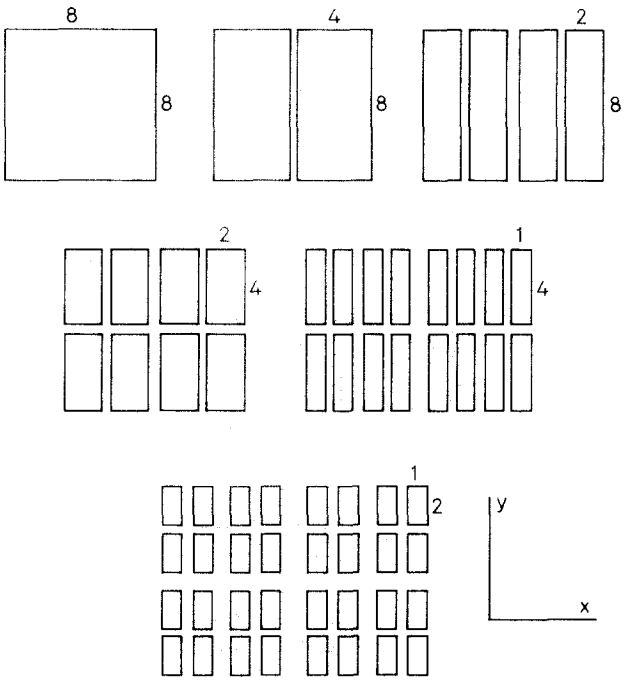

Fig. 6. Numerical example showing development of chocolate tablet boudinage by successive halving of boudins in a flattening type of bulk deformation. In stages (b), (c) & (e) the halving took place by development of extension fractures normal to the x-direction. In (d) and (f) the new fractures are normal to the y-direction. See text for details.

Boudinage under unequal layer-parallel stretching in matrix

Let $\dot{\varepsilon}_x$ and $\dot{\varepsilon}_y$ be the far-field principal strain rates in the matrix. When the brittle plate was circular, a set of extension fractures formed in the major part of the plate more or less at right angles to $\dot{\varepsilon}_x$ (Fig. 5a). Along a narrow peripheral zone the fractures were approximately perpendicular to the periphery. With progressive deformation a second set of fractures started to develop perpendicular to $\dot{\varepsilon}_y$. These experiments show that in a flattening type of bulk deformation, with $\dot{\varepsilon}_x > \dot{\varepsilon}_y > 0$, chocolate tablet structures may form by sequential development of two orthogonal sets of fractures. It is noteworthy that the second set of fractures develops perpendicular to the y-axis although the far-field strain-rate of the matrix is smaller along y than along x. The second set of fractures develop only after the plate had divided into a number of long narrow strips or lenses parallel to the y-axis. Subsequent fractures must develop perpendicular to the long axis of these boudins.

Another series of experiments was performed using long narrow strips of plaster of Paris, with the long axis oriented at 0, 30, 60 and 90° to $\dot{\varepsilon}_x$. Because of the importance of these results, each of the experiments was repeated several times. In each of these experiments a single set of fractures formed perpendicular to the length of the plate (Fig. 5b & c). Thus, the orientation of the fractures was entirely controlled by the geometry of the plate and was independent of the direction of the far-field principal stresses in the matrix. These experiments have a bearing on two aspects of the process of boudinage.

(i) They explain why, in the course of a flattening type of progressive deformation with $\dot{\varepsilon}_x > \dot{\varepsilon}_y > 0$, a second and later set of fractures may develop at right angles to the first, i.e. not perpendicular to the maximum bulk strain rate in the matrix.

(ii) The experiments also have a bearing on the development of chocolate tablet structure in superposed deformations. If a flattening type of deformation is superimposed on a layer which has a set of long, narrow first generation boudins then the second generation boudinage structures are likely to have their axes approximately perpendicular to those of the first set, irrespective of orientations of the principal strain axes in the matrix during the second deformation.

In experiments using anisotropic plates with 'lineations' at angles of 0, 30, 60 and 90° to $\dot{\varepsilon}_x$ in the matrix, two sets of fractures were also produced, one parallel and one at a high angle to the lineation. Let the fractures parallel and perpendicular to the lineations be called longitudinal and transverse fractures. When the lineation was perpendicular to or at an acute angle to $\dot{\varepsilon}_x$, the longitudinal fractures were the first to develop. When the lineation was parallel to $\dot{\varepsilon}_x$ (Figs. 5d and 7c), the first fractures to appear were either longitudinal or transverse, presumably depending upon the ratio of tensile strengths of the plate in the two directions and on the ratio of the far field strain rates $\dot{\varepsilon}_y/\dot{\varepsilon}_x$ in the matrix.

Consider a stretching lineation and a chocolate tablet structure (i) developed successively in the course of a progressive coaxial deformation or (ii) developed in unrelated superposed deformations. If the orientation of extension fractures is indeed controlled by the lineation, then in the first case the longitudinal and

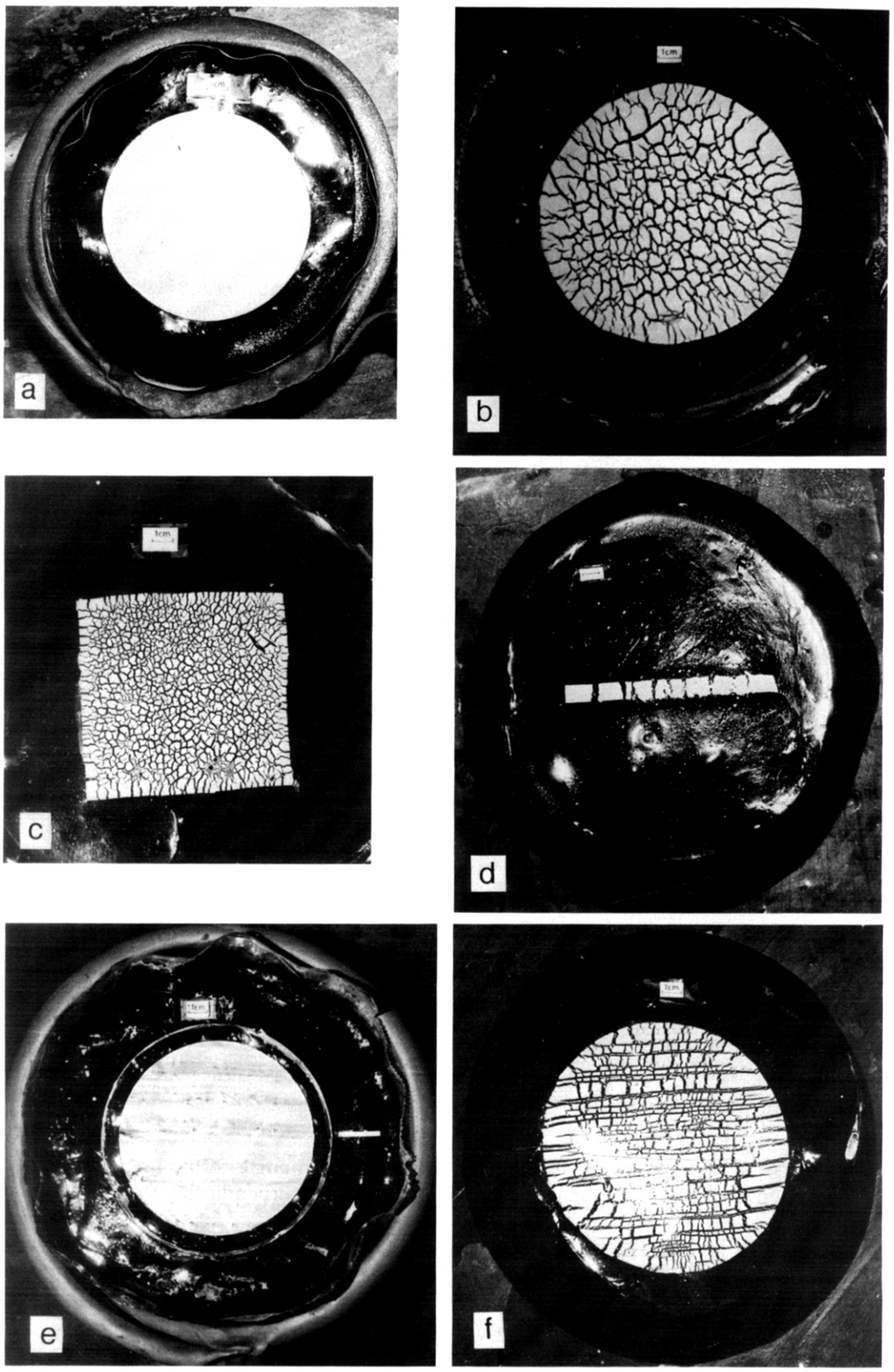

Fig. 4. (a) Top view of pitch model with circular plate of plaster of Paris and side wall of modelling clay. (b) Multi-directional boudinage in circular plate of plaster of Paris in axially symmetric flow of underlying pitch. (c) Multi-directional boudinage of square plate in axially symmetric flow of underlying pitch. (d) Extension fractures transverse to long, narrow plate of plaster of Paris, with axially symmetric flow of underlying pitch. (e) Lineated plate of plaster of Paris on pitch cylinder before start of experiment. (f) Development of extension fractures parallel and perpendicular to lineation in circular plate of plaster of Paris under axially symmetric flow. The fractures parallel to lineation developed first.

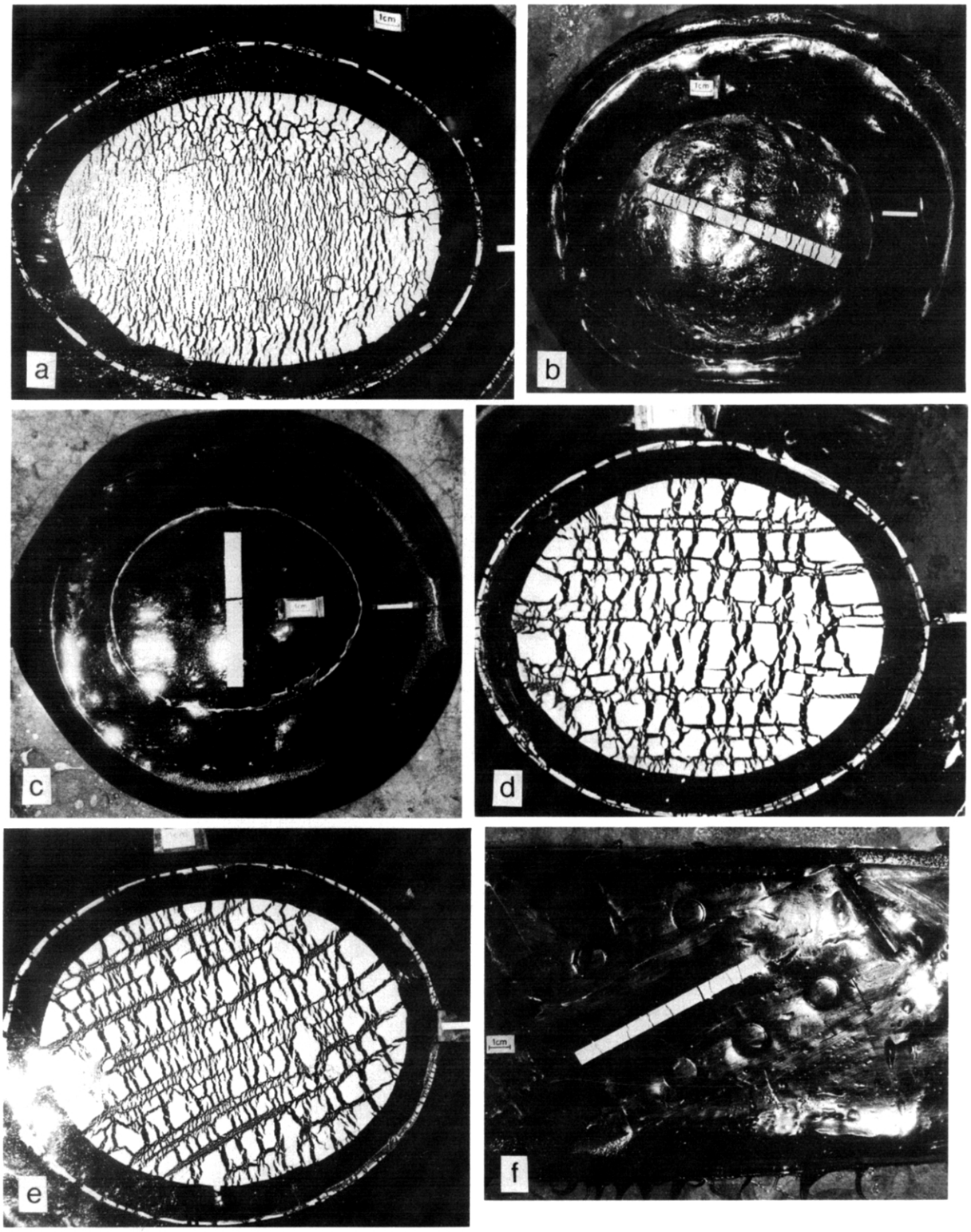

Fig. 5. (a) Circular plate of plaster of Paris subjected to unequal extensions in two directions. The discontinuous outer line was initially a circular marker. The short white line on right-hand side indicates the perpendicular to the long axes of the embedded metal strips. Note incipient development of fractures perpendicular to $\dot{\varepsilon}_y$. (b) Development of transverse fractures in long narrow plate initially oriented at an angle of 30° with $\dot{\varepsilon}_x > \dot{\varepsilon}_y > 0$; note elliptical outline of deformed circular markers. (c) Development of transverse fractures in long, narrow plate resting on pitch cylinder whose upper part is subjected to unequal rates of extension in two directions; note that the fracture is produced perpendicular to $\dot{\varepsilon}_y$. (d) Plaster of Paris plate with brush marks parallel to $\dot{\varepsilon}_x$ showing first set of fractures formed perpendicular to lineation and second set parallel to lineation. The white line on the right is along $\dot{\varepsilon}_x$. (e) Plaster of Paris plate with brush marks at an angle of 30° to $\dot{\varepsilon}_x$; near the upper surface in the pitch slab $\dot{\varepsilon}_x > \dot{\varepsilon}_y > 0$. (f) Development of transverse fractures in a long, narrow plate with the long axis initially at 30° with direction of uniaxial extension (left to right) in matrix. The embossed circular marks on pitch are continually erased by flow of pitch. The photograph shows freshly embossed circular marks.

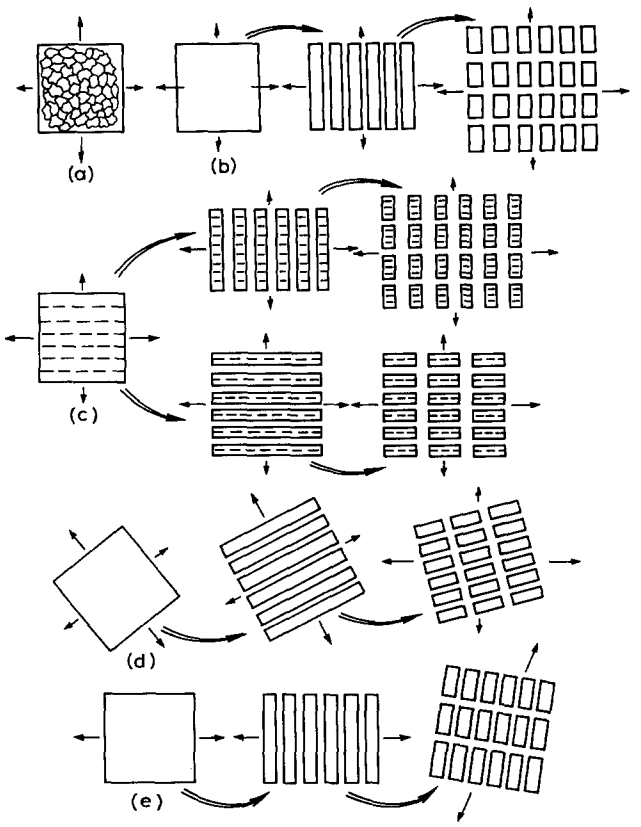

Fig. 7. Schematic representation of different ways of development of chocolate tablet boudinage. Single line arrows indicate far-field layer-parallel strain in matrix. Double line arrows connect an evolutionary sequence. In (a) matrix flow is axially symmetric. (b) and (c) show sequential development of two sets of mutually perpendicular boudins in flattening type of strain with unequal principal extensions. The lower diagram of (c) shows that, in the presence of a strong anisotropy, the first set of boudins may form parallel to a lineation (dashed lines) and normal to $\dot{\varepsilon}_1$. The upper diagram of (c) shows that, if the anisotropy is not so marked, boudinage may take place as in (b). (d) and (e) show development of chocolate tablet boudinage in superposed deformations. In (d) the later deformation is of flattening type and in (e) it causes a uniaxial extension.

transverse boudin axes will be parallel to the directions of principal layer-parallel strains in the matrix (Figs. 5d and 7c). The experimental results indicate that for the second case the boudin axes may not be parallel to the directions of principal layer-parallel strains in the matrix (Figs. 5e and 7d).

Boudinage in long, narrow rectangular plate obliquely aligned in a matrix undergoing uniaxial extension

The long axis of the rectangular plate was aligned at an angle of either 30 or 60° with the direction of extension of the pitch slab. In either case, the extension fractures were normal to the length of the plate (Fig. 5f). In the study of boudinage structures these experiments are relevant in two ways.

(i) Consider the case of superposed boudinage in two unrelated deformations of which the second deformation produces a layer-parallel uniaxial extension of the matrix material. In the general situation this extension will be at some angle to the first generation boudin axes. The experiments suggest that, even in such a situation, the second generation boudin axes will be approximately perpendicular to the first generation axes (Fig. 7e).

(ii) If the brittle layer is mechanically anisotropic, with a lineation neither parallel nor perpendicular to the direction of bulk uniaxial extension, the layer may first break up into a set of long narrow boudins parallel to the lineation. The experiments suggest that, with progressive deformation, a chocolate tablet structure may form by development of a second set of fractures at a high angle to the early boudins.

THEORETICAL CONSIDERATIONS

Although the experimental models give us an insight into the problem of development of chocolate tablet boudinage, they differ from the natural situation in at least one respect. The flow in the viscous material in the experiments is due to the effect of gravity. In the natural situation the ductile flow in the incompetent host is associated with a layer-normal compression. A theoretical analysis has therefore been carried out using a model of an elastic–brittle layer embedded in a viscous matrix (Fig. 8). The sandwiched model is confined between two rigid plates which approach towards each other and give rise to a layer-normal compression. In this theoretical analysis, the details of which are given in the Appendix, three cases have been considered.

(1) The matrix undergoes plane strain in a plane perpendicular to the embedded plate, with unidirectional extension parallel to the plate. The embedded plate is long and narrow and has its long axis at an angle α to the principal extension rate in the matrix (Fig. 9). The stresses in the elastic plate are given by equation (A10). This equation shows that the largest tensile stresses are obtained in the middle of the plate, on a line parallel to the breadth and passing through the centre. At any point on this line the orientation of the principal tensile stress (measured by its angle θ with the long axis

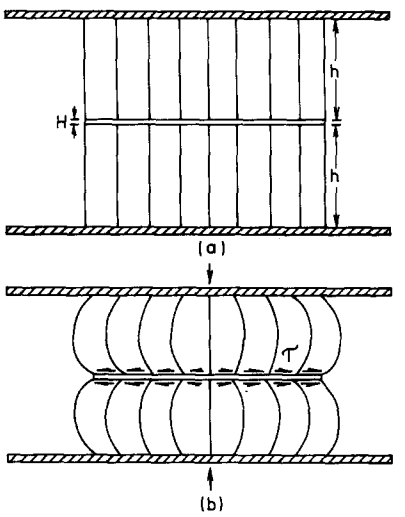

Fig. 8. Development of shear strain in viscous matrix at contact with embedded elastic plate. Lines initially perpendicular to plate in (a) become curved in (b). The shear stress τ at the contact of the plate increases from centre outward and is zero at the centre.

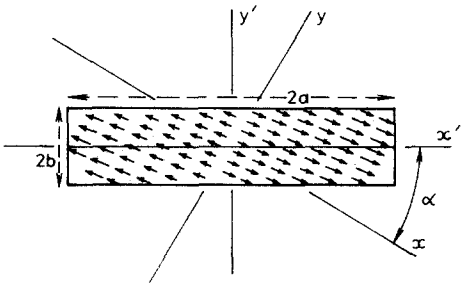

Fig. 9. Plan view of rectangular elastic strip of length $2a$ and breadth $2b$, with schematic representation of external forces imparted by an embedding viscous matrix. x- and y-axes are parallel, respectively, to the mid-level strain rates $\dot{\varepsilon}_x^o$ and $\dot{\varepsilon}_y^o$. x'- and y'-axes are parallel to the length and breadth of the plate, the angle between x and x' being α.

of the plate) is given by equation (A12). This equation and Table A1 show that the principal tensile stress in the middle of the plate is sub-parallel to the long axis of the plate. The extension fracture should therefore form sub-normal to this direction.

(2) The matrix undergoes unequal rates of extension in two directions parallel to the plate, the extension rates at the mid-level of a matrix slab being $\dot{\varepsilon}_x^o > \dot{\varepsilon}_y^o$. The embedded rectangular plate has its edges parallel to these principal directions of matrix strain rates and the principal stresses in the plate are given by equation (A29).

(3) In the third case the bulk deformation is the same as in (2) but the rectangular plate is long and narrow, with the long axis at an angle α to $\dot{\varepsilon}_x^o$. The components of stresses in the plate parallel to its length and breadth, are given by equation (A34). The maximum tensile stresses are obtained in the middle of the plate. The direction of principal stress in the middle of the plate is given by equation (A35). This equation and Table A2 show that if b/a, the ratio of width and length of the plate, is small, i.e. if the plate is long and narrow, the principal tensile stress in the middle is sub-parallel to the long-axis of the plate. This theoretical analysis therefore predicts that the mid-point extension fracture in the plate will be sub-normal to the length of the plate.

DISCUSSION

The following discussion is based on the experimental models and a theoretical analysis of an elastic–brittle layer embedded in a viscous matrix. The stresses and strains in the layer will be different from those in the matrix at a large distance from the layer. It should be understood that the x- and y-axes are directed parallel to the layer and that $\dot{\varepsilon}_x^o$ and $\dot{\varepsilon}_y^o$ are the far-field (mid-level) principal strain rates in the matrix, with $\dot{\varepsilon}_x^o \geq \dot{\varepsilon}_y^o$. The major conclusions are summarized diagrammatically in Fig. 7.

Two-dimensional boudinage structures form in a suitably oriented brittle layer under a flattening type of bulk deformation, with $\dot{\varepsilon}_x^o \geq \dot{\varepsilon}_y^o > 0$. If the strain rates are equal in all directions parallel to the plane of the layer, a network of extension fractures develops more or less simultaneously and divides the layer into boudins which are roundish or polygonal in plan-view (Fig. 7a). However, a large number of two-dimensional boudinage structures show two sets of extension fractures at a high angle to each other. Theoretical and experimental studies indicate that the two sets of fractures could not have formed strictly simultaneously. Such chocolate tablet structures may develop in different ways.

(1) If $\dot{\varepsilon}_x^o > \dot{\varepsilon}_y^o > 0$, a single set of extension fractures will form perpendicular to the x-axis. The width of the boudins will be reduced by successive mid-point fracturing. However, as the experiments and the theoretical studies show, the stress in the embedded layer depends not only on the magnitude of the external force imparted to the layer by the viscous drag of the matrix, but is also controlled by the thickness and layer-length along which the external force acts. Hence, if the boudins formed in the first stage are sufficiently long as compared to their width, the stress along the y-direction or along the long axis of the boudins may become larger than that along the x-direction, even though the far-field strain rate remains larger along the x-axis than along the y-axis (Fig. 7b). Equation (A29) suggests that the course of evolution of chocolate tablet boudinage can be quite complex. After a certain stage of successive mid-point fracturing normal to the x-axis, fractures normal to the y-axis and fractures normal to the x-axis may form in alternate steps until the boudins attain a stable dimension. To clarify this point with a simple numerical example consider an embedded layer 8 units × 8 units square with edges parallel to the x- and the y-axes (Fig. 6a). For the sake of simplicity let us consider only the stresses at the centre of a plate, at $x = y = 0$. According to equation (A29) these stresses are

$$\sigma_x = \frac{Aa^2}{2(1+k)} \qquad \sigma_y = \frac{Akb^2}{2(1+k)}, \tag{1}$$

where a and b are the plate lengths parallel to x- and y-axes, respectively, $k = \dot{\varepsilon}_y^o/\dot{\varepsilon}_x^o$ and A, as given by equation (A1), is a function of matrix viscosity, layer-normal bulk shortening rate and the thicknesses of the brittle plate and embedding viscous slabs. For the numerical example let $k = \frac{1}{10}$. This means that at some distance from the elastic plate the matrix stress along the x-direction is 10 times larger than along the y-direction. By equation (1) we then have at the plate centre

$$\sigma_x = \frac{64A}{2(1+k)} \qquad \sigma_y = \frac{64A}{2(1+k)}$$

so that $\sigma_x = 10\,\sigma_y$. A mid-point fracture will form normal to σ_x if the stress exceeds the tensile strength and will divide the plate into two parts in each of which $a = 4$ and $b = 8$ (Fig. 6b). From equation (1) we find that at the centre of each of these plates $\sigma_x = 2.5\,\sigma_y$. Further fracturing normal to x-axis will give us boudins with $a = 2$ and $b = 8$ (Fig. 6c). Since at the centre of such a boudin $\sigma_y = 1.6\,\sigma_x$, the next set of fractures will form normal to the y-axis, giving rise to boudins with $a = 2$ and $b = 4$ (Fig. 6d). After this stage successive halving of the boudins will take place by fracturing alternately

normal to x-axis and normal to y-axis (Fig. 6e & f) until the boudins have a stable size.

Equation (1) further shows that in exceptional circumstances $\sigma_x = \sigma_y$ in the central part of a boudin, even if $\dot{\varepsilon}_x^o \neq \dot{\varepsilon}_y^o$. Such a situation may develop if during the successive halving, the ratio a/b of the boudins happens to have a critical value, i.e. $a/b = \sqrt{k}$. Under such circumstances the plan-view of a boudinaged layer may show an association of rectangular and roundish outlines.

(2) The development of boudinage will be modified when there is a large difference in the tensile strengths of the layer in different directions. In the present investigation, I have considered the case where the tensile strength of a layer transverse to a lineation is significantly smaller than the strength parallel to the lineation. A similar situation is often encountered in rolled metal plates. During hot or cold working of a two-phase alloy a mechanical fibering develops in the plate due to preferred orientation of deformed second phase grains and preferred fragmentation of grains. This linear structure is similar to the commonly observed stretching lineation in deformed rocks. An important consequence of mechanical fibering is that the strength and ductility of the plate is often lower in the transverse direction than in the longitudinal direction (Dieter 1961, p. 559).

Let us first consider the case in which a stretching lineation and a boudinage structure develop successively in the course of a single continuous deformation with $\dot{\varepsilon}_x^o > \dot{\varepsilon}_y^o > 0$. The lineation will initiate parallel to the x-axis. In such a lineated rock the first set of extension fractures will develop perpendicular to either σ_x or σ_y (Fig. 7c); this will depend on the ratio $\dot{\varepsilon}_y^o/\dot{\varepsilon}_x^o$ as well as on the ratio of tensile strengths perpendicular and parallel to the lineation. In either case, if a second set of fractures develops it will be at right angles to the first set (Fig. 7c).

(3) If the lineation and the boudinage structure develop successively in two unrelated deformations, the lineation may not be parallel to the far-field principal strain rate of the second deformation. If the tensile strength perpendicular to the lineation is much lower than that parallel to the lineation, then, for a flattening type of bulk deformation, either with $\dot{\varepsilon}_x^o = \dot{\varepsilon}_y^o$ or with $\dot{\varepsilon}_x^o > \dot{\varepsilon}_y^o$ the first set of extension fractures will be parallel to the lineation and the second set will subsequently form normal to the first. In general, neither set will be parallel to the far-field principal strain of the second deformation (Fig. 7d).

No experiments were performed with similar lineated layers in bulk uniaxial extension. However, the general principles which emerge from this study lead to the conclusion that even for such a bulk uniaxial extension, with $\dot{\varepsilon}_x^o > 0$, $\dot{\varepsilon}_y^o = 0$, chocolate tablet boudinage, with boudin axes parallel and perpendicular to the lineation, can develop, provided the lineation is at an angle to the principal strain rate in the matrix.

(4) In all three cases described above, the chocolate tablet boudinage formed during a single progressive deformation. An important conclusion which emerges from the experimental and theoretical studies is that, even if two events of unidirectional boudinage are superposed on one another by unrelated deformations, there is a strong likelihood that the two sets of boudin axes or neck lines will be more or less at right angles to each other (Fig. 7e). This is the only relation to be expected when the first generation boudins are very much longer than their width and the process of second generation boudinage is not modified by the development of a strong second generation anisotropy. In general, the orientation of the second generation boudin axis will be oblique to the second generation principal strain axes in the incompetent host.

The models presented here refer to certain simple situations. The mode of development of chocolate tablet boudinage may be modified by other factors, such as the presence of flaws and inhomogeneities, the presence of a cleavage transecting the layer or the development of a second generation lineation. Under the influence of such modifying factors the two sets of boudin axes, either in progressive deformation or in superposed deformations, may not be at a high angle to each other. Moreover, the present analysis is essentially concerned with the development of two-dimensional boudinage in elastic–brittle layers in which there is no pre- or post-boudinage plastic deformation. In cases of progressive non-coaxial deformation or during superposed deformations the angle between two sets of boudin axes may be modified by plastic deformation.

As mentioned in the introduction, lineated rocks in certain areas show both boudinage and pinch-and-swell structures, with the boudin axes running parallel to the lineation and the neck lines of pinch-and-swell at a high angle to the lineation. Such a difference in behaviour may result from different strain rates parallel and perpendicular to the lineation. Alternatively, the occurrence of such structures might suggest that, as in the case of certain rolled and lineated metal sheets, the ductility of the rocks was higher in the longitudinal direction than in the transverse direction. As a consequence, in a flattening type of bulk deformation the rock may develop extension fractures in one direction while ductile flow in the other direction may give rise to pinch-and-swell structures.

Certain aspects of the present work need further elaboration.

(1) In both the experiments and the theoretical studies the competent layer lies parallel to the $\lambda_1\lambda_2$-plane of bulk strain of the matrix. Evidently, further work is necessary for the more general situation in which the layer is inclined to all the principal axes of bulk strain.

(2) The experiments show that, in an elastic–brittle layer, boudinage takes place sequentially by successive mid-point fracturing. However, when there was a large amount of permanent deformation before fracturing, the extension fractures formed all over the layer more or less at the same time. Although the latter observation is of considerable importance, the reason for such simultaneous boudinage is not immediately apparent. There is a possibility that the latter type of boudinage takes places as a consequence of simultaneous pinching-

and-swelling, as predicted by Smith (1975, 1977). There is no way of testing this hypothesis from the present series of experiments in which the plates of plaster of Paris are too thin for identifying incipient pre-fracture pinch-and-swell structures.

(3) Chocolate tablet structures in lineated rocks may form by development of two sets of extension fractures parallel and perpendicular to a lineation. In some areas the fractures parallel to a stretching lineation are more prominent than those perpendicular to it. The experiments with lineated sheets suggest that, in such rocks, an initial set of boudins may more easily form parallel to the lineations than in any other direction, even if the maximum rate of extension in the rock is not at right angles to the lineation. The importance of this process, or the lack of it, can be assessed only after more extensive studies with natural examples of chocolate tablet structures. The method of study devised by Casey *et al.* (1983) may offer valuable information in this context.

Acknowledgements—The author wishes to thank N. Mandal and S. Karmakar for their help with the experiments. The critical comments by W. D. Means and M. B. Bayly and the reviews by D. J. Sanderson, W. M. Schwerdtner and G. E. Lloyd helped to improve the final manuscript.

REFERENCES

Casey, M., Dietrich, D. & Ramsay, J. G. 1983. Methods of determining deformation history for chocolate tablet boudinage with fibrous crystals. *Tectonophysics* **92**, 211–239.

Coe, K. 1959. Boudinage structure in West Cork, Ireland. *Geol. Mag.* **96**, 192–200.

Dieter, G. E. 1976. *Mechanical Metallurgy*. McGraw-Hill, New York.

Fyson, W. K. 1962. Tectonic structures in the Devonian rocks near Plymouth, Devon. *Geol. Mag.* **99**, 208–226.

Ghosh, S. K. & Ramberg, H. 1976. Reorientation of inclusions by combination of pure shear and simple shear. *Tectonophysics* **34**, 1–70.

Ghosh, S. K. & Sengupta, S. 1987. Structural history of the Singhbhum Shear Zone in relation to the northern folded belt. In: *Geological Evolution of Peninsular India—Petrological and Structural Aspects* (edited by Saha, A. K.). Hindustan Publishing Corporation, New Delhi.

Jaeger, J. C. 1964. *Elasticity, Fracture and Flow*. Methuen & Co., London.

Lloyd, G. E. & Ferguson, C. C. 1981. Boudinage structure—some new interpretations based on elastic–plastic finite element simulations. *J. Struct. Geol.* **3**, 117–128.

Lloyd, G. E., Ferguson, C. C. & Reading, K. 1982. A stress transfer model for the development of extension fracture boudinage. *J. Struct. Geol.* **4**, 355–372.

Naha, K. & Halyburton, R. V. 1977. Structural pattern and strain history of superposed fold system in the Precambrian of Central Rajasthan, India, Parts I & II. *Precambrian Res.* **4**, 39–84, 85–111.

Ramberg, H. 1955. Natural and experimental boudinage and pinch-and-swell structures. *J. Geol.* **63**, 512–526.

Ramsay, J. G. 1967. *Folding and Fracturing of Rocks*. McGraw-Hill, New York.

Sanderson, D. J. 1974. Patterns of boudinage and apparent stretching lineation developed in folded rocks. *J. Geol.* **82**, 651–661.

Schwerdtner, W. M. & Clark, A. R. 1967. Structural analysis of Mokka Fiord and South Fiord domes, Axel Heiberg Island, Canadian Arctic. *Can. J. Earth Sci.* **4**, 1229–1245.

Smith, R. B. 1975. Unified theory of onset of folding, boudinage and mullion structure. *Bull. geol. Soc. Am.* **86**, 1601–1609.

Smith, R. B. 1977. Formation of folds, boudinage and mullions in non-Newtonian materials. *Bull. geol. Soc. Am.* **88**, 312–320.

Symon, K. R. 1963. *Mechanics*. Addison-Wesley, Reading, Massachusetts.

Timoshenko, S. & Goodier, J. N. 1951. *Theory of Elasticity*. McGraw-Hill, New York.

Wegmann, C. E. 1932. Note sur le boudinage. *Bull. Soc. geol. Fr.*, 5 *Ser.* **II**, 477–489.

APPENDIX

GENERAL

In the following theoretical analysis it is assumed that a thin elastic–brittle plate of thickness H is sandwiched between two thick viscous slabs, each of thickness h (Fig. 8). The sandwiched model is confined between two rigid plates, which approach towards the embedded plate with velocities $\pm \dot{w}$.

Ramberg has considered the development of boudinage when the viscous matrix is undergoing a unidirectional extension along the long axis of a rectangular elastic plate. If there is no slip between the matrix and the plate and its two confining walls, layer-normal marker lines in the matrix will bend outward symmetrically (Fig. 8). At the contact with the embedded plate, the marker lines on either side of the symmetry plane, will no longer remain perpendicular to the surface of the embedded plate. The contact shear strain and shear stress in the matrix will be zero in the middle of the plate and will increase towards either end. From the symmetry of distribution of this shear stress τ (Fig. 8), it is evident that under its action the elastic plate will be subjected to an external force of magnitude $2\tau/H$ per unit volume of the plate (Ramberg 1955, Lloyd *et al.* 1982). The magnitude of this force will be

$$R_x = A, \qquad R_y = 0 \tag{A1}$$

with

$$A = \frac{12\eta \dot{w}_0}{Hh^2} \text{ (Ramberg 1955)},$$

where η is the coefficient of viscosity in the matrix and $\dot{w}_0$ is the upward velocity of a rigid plate. It is noteworthy that, since R_x is an external force which acts on unit volume, it has the nature of body force density (Symon 1960, p. 246). Although Ramberg's analysis is for a rectangular plate the long axis of which is parallel to the unidirectional extension in the matrix, it will be assumed in the following analysis that equation (A1) holds, at least as a first approximation, to rectangular plates, the normal to which is parallel to $\dot{w}_0$, but the long axis of which is at an acute angle to the far-field principal strain rate along the x-direction in the matrix (Fig. 9).

BOUDINAGE IN OBLIQUE STRIP UNDER BULK UNIAXIAL EXTENSION

Let us consider the stress distribution in an elastic strip embedded in a viscous matrix undergoing a layer-normal compression along the z-axis and a unidirectional extension along the x-axis (Fig. 9). The origin of co-ordinates is chosen at the centre of the elastic strip which has length $2a$ and width $2b$ on the xy-plane. The long axis of the plate is oriented at an angle α with the x-axis. If the plate is very long compared to its width it will rotate in the xy-plane as a similarly oriented passive marker line in the matrix (Ghosh & Ramberg 1976).

Let x' and y' co-ordinate axes be chosen along the length and the width of the plate, and with the origin at the centre. The angle between x and x' is α. From the symmetry of the external forces R_x about the centre (Fig. 9) it may be inferred that the displacements u' and v' corresponding to the x', y' co-ordinates are antisymmetric about the origin. In other words u' and v' are odd functions of x' and y':

$$u'(-x', -y') = -u'(x', y')$$
$$v'(-x', -y') = -v'(x', y').$$

Let us introduce a simplifying assumption that the longitudinal strain $\varepsilon_{x'}$ is the same at all points in a cross-section parallel to the width and that $\varepsilon_{y'}$ remains the same at all points on a section parallel to the length of the plate. The components of displacement can then be represented by the following expressions

$$u' = a_1 x'^3 + a_2 x' + a_3 y'^2 - \omega y'$$
$$v' = a_4 x'^2 + a_5 x' + a_6 y'^3 + \omega x', \tag{A2}$$

where a_1, a_2, etc., are undetermined constants and ω is a rigid rotation which does not enter in the computation of stresses and strains. The

antisymmetry of the displacements implies that (A2) cannot have terms containing $x'y'$ and $x'^2y'^2$, while from the condition that $\varepsilon_{x'}$ does not vary along the width and $\varepsilon_{y'}$ does not vary along the length of the plate we find that the displacement functions cannot have terms with x'^2y' and $x'y'^2$.

From (A2) the strains are expressed as

$$\begin{aligned}\varepsilon_{x'} &= \frac{\partial u'}{\partial x'} = 3a_1x'^2 + a_2\\ \varepsilon_{y'} &= \frac{\partial v'}{\partial y'} = 3a_6y'^2 + a_5\\ \gamma_{x'y'} &= \frac{\partial v'}{\partial x'} + \frac{\partial u'}{\partial y'} = 3(a_4x'^2 + a_3y'^2).\end{aligned} \tag{A3}$$

For plane stress (Timoshenko & Goodier 1951, p. 24) within the plate the stresses are:

$$\begin{aligned}\sigma_{x'} &= \frac{E}{1-\nu^2}(3a_1x'^2 + 3\nu a_6y'^2 + a_2 + \nu a_5)\\ \sigma_{y'} &= \frac{E}{1-\nu^2}(3a_1\nu x'^2 + 3a_6y'^2 + \nu a_2 + a_5)\\ \tau_{x'y'} &= \frac{3E}{2(1+\nu)}(a_4x'^2 + a_3y'^2),\end{aligned} \tag{A4}$$

where ν is Poisson's ratio.

For a long narrow strip the stresses normal to the boundary should vanish at least at the tips of the long and the short axes of the plate, i.e.

$$\begin{aligned}\sigma_{x'} &= 0 \quad \text{at } x' = a,\ y' = 0,\\ \sigma_{y'} &= 0 \quad \text{at } x' = 0,\ y' = b.\end{aligned}$$

Substituting these boundary conditions in (A4) we find

$$\begin{aligned}3a_1a^2 + (a_2 + \nu a_5) &= 0\\ 3a_6b^2 + (\nu a_2 + a_5) &= 0\end{aligned}$$

or

$$\begin{aligned}a_2 &= \frac{3}{1-\nu^2}(\nu a_6b^2 - a_1a^2)\\ a_5 &= \frac{3}{1-\nu^2}(\nu a_1a^2 - a_6b^2).\end{aligned} \tag{A5}$$

The stresses given by (A4) can therefore be expressed as

$$\begin{aligned}\sigma_{x'} &= \frac{E}{1-\nu^2}[3a_1(x'^2 - a^2) + 3\nu a_6y'^2]\\ \sigma_{y'} &= \frac{E}{1-\nu^2}[3\nu a_1x'^2 + 3a_6(y'^2 - b^2)]\\ \tau_{x'y'} &= \frac{3E}{2(1+\nu)}(a_4x'^2 + a_3y'^2).\end{aligned} \tag{A6}$$

The body force per unit volume in the plate as given by (A1) has components along the x'- and y'-axes,

$$\begin{aligned}R_{x'} &= R_x\cos\alpha + R_y\sin\alpha\\ R_{y'} &= -R_x\sin\alpha + R_y\cos\alpha.\end{aligned}$$

Since $R_y = 0$ and $R_x = Ax$,

$$\begin{aligned}R_{x'} &= A\cos^2\alpha.x' - A\sin\alpha\cos\alpha.y'\\ R_{y'} &= -A\sin\alpha\cos\alpha.x' + A\sin^2\alpha.y'.\end{aligned} \tag{A7}$$

It should be noted that in deriving these equations, α was taken as the angle between the unprimed and the primed co-ordinates and not the other way round.

From the elastic equation of equilibrium (Timoshenko & Goodier 1951),

$$\begin{aligned}\frac{\partial\sigma_{x'}}{\partial x'} + \frac{\partial\tau_{x'y'}}{\partial y'} + R_{x'} &= 0\\ \frac{\partial\sigma_{y'}}{\partial y'} + \frac{\partial\tau_{x'y'}}{\partial x'} + R_{y'} &= 0\end{aligned} \tag{A8a}$$

and from equations (A6) and (A7) we have

$$\begin{aligned}\left(\frac{6Ea_1}{1-\nu^2} + A\cos^2\alpha\right)x' + \left(\frac{3Ea_3}{1+\nu} - A\sin\alpha\cos\alpha\right)y' &= 0\\ \left(\frac{3Ea_4}{1+\nu} - A\sin\alpha\cos\alpha\right)x' + \left(\frac{6Ea_6}{1-\nu^2} + A\sin^2\alpha\right)y' &= 0.\end{aligned} \tag{A8b}$$

In each of these equations, for the right-hand side to be zero, the coefficients of x' and y' must separately be zero. All the coefficients of the displacement functions, as given by (A2), are thus determined from equations (A5) and (A8b):

$$\begin{aligned}a_1 &= \frac{-(1-\nu^2)}{6E}A\cos^2\alpha\\ a_2 &= \frac{A}{2E}(a^2\cos^2\alpha + b^2\nu\sin^2\alpha)\\ a_3 = a_4 &= \frac{1+\nu}{3E}A\sin\alpha\cos\alpha\\ a_5 &= \frac{A}{2E}(a^2\nu\cos^2\alpha + b^2\sin^2\alpha)\\ a_6 &= \frac{-(1-\nu^2)}{6E}A\sin^2\alpha.\end{aligned} \tag{A9}$$

The stresses are found from (A6) and (A9) as:

$$\begin{aligned}\sigma_{x'} &= \frac{A}{2}[(a^2 - x'^2)\cos^2\alpha - \nu\sin^2\alpha.y'^2]\\ \sigma_{y'} &= \frac{A}{2}[(b^2 - y'^2)\sin^2\alpha - \nu\cos^2\alpha.x'^2]\\ \tau_{x'y'} &= \frac{A}{2}\sin\alpha\cos\alpha\,(x'^2 + y'^2).\end{aligned} \tag{A10}$$

For any point (x', y') the directions of principal stresses (Jaeger 1964, p. 7) are given by the relation

$$\tan 2\theta = \frac{\sin 2\alpha(x'^2 + y'^2)}{[\{(a^2 - x'^2)\cos^2\alpha - (b^2 - y'^2)\sin^2\alpha\} + \nu(\cos^2\alpha.x'^2 + \sin^2\alpha.y'^2)]}. \tag{A11}$$

From (A10) and (A11) it is evident that the maximum value of the tensile stress is obtained at points along the line $x' = 0$. Along such a line let us express y' as a fraction of b, i.e. $y' = cb$, where c ranges from 0 to 1. The directions of principal stresses are given by the relation

$$\tan 2\theta = \frac{\sin 2\alpha.c^2b^2}{a^2\cos^2\alpha - b^2(1-c^2)\sin^2\alpha - \nu\sin^2\alpha.c^2b^2}.$$

Dividing the numerator and denominator by a^2, we find

$$\tan 2\theta = \frac{c^2\left(\frac{b}{a}\right)^2\sin 2\alpha}{\cos^2\alpha - \left(\frac{b}{a}\right)^2\sin^2\alpha(1 + \nu c^2 - c^2)}. \tag{A12}$$

Equation (A12) shows that θ will tend to zero as b/a tends to zero. Thus, for slender strips with a much larger than b, $\theta \approx 0$, provided $\alpha \neq 90°$. For all values of b/a, θ is zero at the centre of strip, at $x' = y' = 0$. The values of θ for $b/a = 1/10$ are shown in Table A1 for α as 30, 60 and 80°. θ remains very small unless α is close to 90° and a/b is small. When the stresses exceed the tensile strength of a long narrow plate, the tension fracture should therefore form essentially normal to the plate length, irrespective of the angle α (with $\alpha \neq 90°$) between the long axis of the plate and the direction of far-field tensile stress in the viscous matrix.

Table A1. Direction of maximum tensile stress for uniaxial extension at points on short axis of plate. $b/a = \frac{1}{10}$, $\nu = \frac{1}{3}$. Values of θ are given in degrees

Position of points	For α = 30°	60°	80°
$x = 0$, $y = 0$	0	0	0
$x = 0$, $y = \frac{1}{4}b$	0.02	0.06	0.29
$x = 0$, $y = \frac{1}{2}b$	0.08	0.26	1.11
$x = 0$, $y = \frac{3}{4}b$	0.19	0.57	2.28
$x = 0$, $y = b$	0.33	1.00	3.60

BOUDINAGE UNDER UNEQUAL LAYER-PARALLEL EXTENSION OF MATRIX

Rectangular plate symmetrically oriented with respect to flow in the matrix

The co-ordinate axes x and y are chosen on the upper surface of the plate, with the z-axis directed upward and with the origin at the centre of the upper face of the elastic plate. Since the flow in the matrix is symmetrical in the upper and the lower viscous slabs, it is sufficient to consider only the upper slab. The flow is not necessarily axially symmetric as in Ramberg's (1955) model of two-dimensional boudinage. Rather, the far-field matrix strain rates $\dot{\varepsilon}_x^0$ and $\dot{\varepsilon}_y^0$, say at $z = h/2$, are taken as unequal in the general situation. The solution of the problem has been made mainly by representing the velocities $\dot{u}$, $\dot{v}$ and $\dot{w}$ through polynomials with unknown coefficients. The general forms of the polynomials are chosen to be consistent with the symmetry of the flow and with the condition that the viscous material adheres to the rigid plates at $z = 0$ and $z = h$. In particular, since a marker line parallel to the xy-plane continues to remain parallel to the xy-plane, $\dot{w}$ and $\dot{\varepsilon}_z$ must be independent of x and y and are functions of z only. The no-slip condition implies that $\dot{u} = \dot{v} = \dot{w} = \dot{\varepsilon}_x = \dot{\varepsilon}_y = \dot{\varepsilon}_z = 0$ at $z = 0$. It is also known that $-\dot{u}(x) = \dot{u}(-x)$ and $-\dot{v}(y) = \dot{v}(-y)$, with $\dot{u} = 0$ at $x = 0$ and $\dot{v} = 0$ at $y = 0$. An additional assumption is made that the longitudinal strain rates parallel to the x and the y axes are constant at all points on a plane parallel to the xy-plane. This implies that $\dot{\varepsilon}_x$ and $\dot{\varepsilon}_y$ are functions of z only. The following expressions for the velocities in the matrix are consistent with these conditions.

$$\begin{aligned} \dot{u} &= a_1xz^2 + a_2xz \\ \dot{v} &= a_3yz^2 + a_4yz \\ \dot{w} &= a_5z^3 + a_6z^2, \end{aligned} \tag{A13}$$

where a_1, a_2, etc., are unknown constants.

The rates of longitudinal strains are:

$$\begin{aligned} \dot{\varepsilon}_x &= \frac{\partial \dot{u}}{\partial x} = a_1z^2 + a_2z \\ \dot{\varepsilon}_y &= \frac{\partial \dot{v}}{\partial y} = a_3z^2 + a_4z \\ \dot{\varepsilon}_z &= \frac{\partial \dot{w}}{\partial z} = 3a_5z^2 + 2a_6z. \end{aligned} \tag{A14}$$

The rates of shear strains are:

$$\begin{aligned} \dot{\gamma}_{xz} &= \frac{\partial \dot{w}}{\partial x} + \frac{\partial \dot{u}}{\partial z} = 2a_1xz + a_2x \\ \dot{\gamma}_{yz} &= \frac{\partial \dot{w}}{\partial y} + \frac{\partial \dot{v}}{\partial z} = 2a_3yz + a_4y \\ \dot{\gamma}_{xy} &= \frac{\partial \dot{v}}{\partial x} + \frac{\partial \dot{u}}{\partial y} = 0. \end{aligned} \tag{A15}$$

By substituting the expressions for the strain rates in the continuity equation for incompressible flow, $\dot{\varepsilon}_x + \dot{\varepsilon}_y + \dot{\varepsilon}_z = 0$, we find, after simplification

$$(a_1 + a_3 + 3a_5)z + (a_2 + a_4 + 2a_6) = 0. \tag{A16}$$

Equation (A16) leads us to the following inter-relations among the coefficients of (A13):

$$\begin{aligned} a_1 + a_3 + 3a_5 &= 0 \\ a_2 + a_4 + 2a_6 &= 0. \end{aligned} \tag{A17}$$

Three other inter-relations are obtained by imposing the boundary condition that at $z = h$, $\dot{u} = \dot{v} = 0$ and $\dot{w} = -\dot{w}_0$, recalling that the upper and the lower confining plates move with a velocity $-\dot{w}_0$ and $\dot{w}_0$, respectively.

$$\begin{aligned} a_1h + a_2 &= 0 \\ a_3h + a_4 &= 0 \\ a_5h + a_6 &= -\frac{\dot{w}_0}{h^2}. \end{aligned} \tag{A18}$$

Let

$$\frac{\dot{\varepsilon}_x^0}{\dot{\varepsilon}_y^0} = k, \tag{A19}$$

where k is a constant ranging between 0 and 1. It may be recalled that $\dot{\varepsilon}_x^0$ and $\dot{\varepsilon}_y^0$ are the mid-level strain rates at $z = h/2$. From (A14) and (A19) we find

$$a_3h + 2a_4 - kha_1 - 2ka_2 = 0. \tag{A20}$$

The coefficients a_1–a_6 are determined by solving the six equations given by (A17), (A18) and (A20).

$$\begin{aligned} a_1 &= -\frac{1}{(1+k)}\cdot\frac{6\dot{w}_0}{h^3}, & a_2 &= \frac{1}{(1+k)}\frac{6\dot{w}_0}{h^2}, \\ a_3 &= -\frac{k}{(1+k)}\cdot\frac{6\dot{w}_0}{h^3}, & a_4 &= \frac{k}{(1+k)}\frac{6\dot{w}_0}{h^2}, \\ a_5 &= \frac{2\dot{w}_0}{h^3}, & a_6 &= -\frac{3\dot{w}_0}{h^2}. \end{aligned} \tag{A21}$$

The strain rates in the viscous matrix can be determined from (A14), (A15) and (A21). For the present purpose it is sufficient to determine the shear strain rates $\dot{\gamma}_{xz}$ and $\dot{\gamma}_{yz}$ on the upper face of the elastic plate, i.e. on the surface $z = 0$.

$$\begin{aligned} \dot{\gamma}_{xz} &= \frac{1}{(1+k)}\frac{6\dot{w}_0x}{h^2} \\ \dot{\gamma}_{yz} &= \frac{k}{(1+k)}\frac{6\dot{w}_0y}{h^2}. \end{aligned} \tag{A22}$$

The corresponding shear stresses are

$$\begin{aligned} \tau_{xz} &= \frac{1}{(1+k)}\frac{6\eta\dot{w}_0x}{h^2} \\ \tau_{yz} &= \frac{k}{(1+k)}\frac{6\eta\dot{w}_0y}{h^2}. \end{aligned} \tag{A23}$$

The viscous slabs impart the same stresses on the lower face of the elastic plate. The force per unit volume along the middle surface of the plate can therefore be represented by its two components

$$\begin{aligned} R_x &= \frac{1}{(1+k)}Ax \\ R_y &= \frac{k}{(1+k)}Ay, \end{aligned} \tag{A24}$$

where

$$A = \frac{12\eta\dot{w}_0}{Hh^2}.$$

To determine the stresses in the middle plane of the plate we may represent the displacements $u(x, y)$ and $v(x, y)$ by similar expressions as in (A2). Since in this case the long and the short axes of the rectangular plate are along the x- and y-axes, respectively, there is no rigid rotation of the plate. Moreover, there is no necessity to determine the displacements with reference to the primed co-ordinates.

$$\begin{aligned} u &= a_1x^3 + a_2x + a_3y^3 \\ v &= a_4x^3 + a_5y + a_6y^3, \end{aligned} \tag{A25}$$

where a_1, a_2, etc., are not necessarily the same as in (A2). The general expressions for stresses and strains are the same as in (A3), (A4) and (A6). However, in this case, with the long and short axes aligned parallel to the directions of the far-field principal strain rates in the matrix, the shear stress, τ_{xy} should vanish, at least along the lines $y = 0$ and $x = 0$. From (A4) we then find that

$$a_2 = a_4 = 0.$$

The stresses as given by (A6) can then be written as

$$\begin{aligned} \sigma_x &= \frac{E}{1-\nu^2}[3a_1(x^2 - a^2) + 3\nu a_6y^2] \\ \sigma_y &= \frac{E}{1-\nu^2}[3\nu a_1x^2 + 3a_6(y^2 - b^2)] \\ \tau_{xy} &= 0. \end{aligned} \tag{A26}$$

From (A8a), (A24) and (A26), we find

$$\begin{aligned} \left(\frac{6Ea_1}{1-\nu^2} + \frac{A}{1+k}\right)x &= 0 \\ \left(\frac{6Ea_6}{1-\nu^2} + \frac{kA}{1+k}\right)y &= 0 \end{aligned} \tag{A27}$$

or

$$\begin{aligned} a_1 &= \frac{-A(1-\nu^2)}{6E(1+k)} \\ a_6 &= \frac{-kA(1-\nu^2)}{6E(1+k)}. \end{aligned} \tag{A28}$$

Substituting the expressions for a_1 and a_6 in (A26), we find, after simplification, the principal stresses directed parallel to x- and y-axes:

$$\sigma_x = \frac{A}{2(1+k)}[(a^2 - x^2) - \nu k y^2]$$
$$\sigma_y = \frac{A}{2(1+k)}[k(b^2 - y^2) - \nu x^2]. \quad \text{(A29)}$$

The maximum value of σ_x is at $x = 0$. Along the line $x = 0$, σ_x decreases with increasing y. Hence, if σ_x exceeds the tensile strength of the plate, the mid-point extension fracture will form at the centre at a right angle to the plate length and, with increasing σ_x, will cut across the entire width of the plate.

Rectangular plate asymmetrically oriented with respect to the flow in the matrix

Consider next a long narrow rectangular plate lying on the xy-plane and with the long axis oriented at an angle α with the x-axis. As in the first case, an approximate solution of this problem can be obtained if we assume that the viscous drag on the plate gives rise to a force per unit volume on the middle surface of the plate and that the components R_x and R_y of the force are given by (A24).

Let us choose a new set of co-ordinate axes on the middle surface of the plate, with x' and y' aligned along the long and the short axes. For reasons similar to those given for the first case, the displacements may be represented as in (A2):

$$u' = a_1 x'^3 + a_2 x' + a_3 y'^3 - \omega y'$$
$$v' = a_4 x'^3 + a_5 y' + a_6 y'^3 + \omega x'. \quad \text{(A30)}$$

The coefficients a_1, a_2, etc., are not necessarily the same as in (A2) or (A25).

From (A24) we have

$$R_x = \frac{1}{1+k} Ax, \qquad R_y = \frac{k}{1+k} Ay.$$

The components along the x'- and y'-axes are

$$R_{x'} = R_x \cos\alpha + R_y \sin\alpha = \frac{A}{1+k}(x\cos\alpha + ky\sin\alpha)$$
$$R_{y'} = -R_x \sin\alpha + R_y \cos\alpha = \frac{A}{1+k}(-x\sin\alpha + ky\cos\alpha)$$

or

$$R_{x'} = \frac{A}{1+k}[(\cos^2\alpha + k\sin^2\alpha)x' + (k-1)\sin\alpha\cos\alpha . y'] \quad \text{(A31)}$$
$$R_{y'} = \frac{A}{1+k}[(k-1)\sin\alpha\cos\alpha . x' + (\sin^2\alpha + k\cos^2\alpha)y'].$$

Substituting the expressions for $\sigma_{x'}$, $\sigma_{y'}$, $\tau_{x'y'}$, $R_{x'}$ and $R_{y'}$ from equations (A6) and (A31) into the equilibrium equation (A8a), we find that

$$\left[\frac{6Ea_1}{1-\nu^2} + \frac{A}{1+k}(\cos^2\alpha + k\sin^2\alpha)\right]x' + \left[\frac{3Ea_3}{1+\nu} + \frac{A(k-1)}{1+k}\sin\alpha\cos\alpha\right]y' = 0$$
$$\left[\frac{A(k-1)}{1+k}\sin\alpha\cos\alpha + \frac{3Ea_4}{1+\nu}\right]x' + \left[\frac{6Ea_6}{1-\nu^2} + \frac{A}{1+k}(\sin^2\alpha + k\cos^2\alpha)\right]y' = 0. \quad \text{(A32)}$$

In each of these equations, for the right-hand side to be zero, the coefficients of x' and y' must be zero. Therefore,

Table A2. Direction of maximum tensile stress for biaxial extension at points on short axis of plate. $b/a = \frac{1}{10}$, $\nu = \frac{1}{3}$, $\dot{\varepsilon}_x^0 = \dot{\varepsilon}_y^0$. Values of θ are given in degrees

Position of points	For α = 30°	60°	80°
$x = 0$, $y = 0$	0	0	0
$x = 0$, $y = \frac{1}{4}b$	0.009	0.01	0.006
$x = 0$, $y = \frac{1}{2}b$	0.04	0.05	0.02
$x = 0$, $y = \frac{3}{4}b$	0.08	0.11	0.05
$x = 0$, $y = b$	0.14	0.20	0.10

$$a_1 = -\frac{A(1-\nu^2)}{6E(1+k)}(\cos^2\alpha + k\sin^2\alpha)$$
$$a_3 = a_4 = -\frac{A(k-1)(1+\nu)}{3E(1+k)}\sin\alpha\cos\alpha \quad \text{(A33)}$$
$$a_6 = -\frac{A(1-\nu^2)}{6E(1+k)}(\sin^2\alpha + k\cos^2\alpha),$$

a_2 and a_5 are then obtained from equation (A5). The stresses, as obtained after substitution of the expressions for a_1, a_3, a_4 and a_6 in equation (A6), are

$$\sigma_{x'} = \frac{A}{2(1+k)}[(\cos^2\alpha + k\sin^2\alpha)(a^2 - x'^2) - \nu(\sin^2\alpha + k\cos^2\alpha)y'^2]$$
$$\sigma_{y'} = \frac{A}{2(1+k)}[(\sin^2\alpha + k\cos^2\alpha)(b^2 - y'^2) - \nu(\cos^2\alpha + k\sin^2\alpha)x'^2] \quad \text{(A34)}$$
$$\tau_{x'y'} = \frac{A(1-k)}{2(1+k)}\sin\alpha\cos\alpha\,(x'^2 + y'^2).$$

The maximum value of $\sigma_{x'}$ is obtained on the line $x' = 0$. Along that line let us express y' as a fraction of b, i.e. $y' = cb$, where c ranges between 0 and 1. The directions of the principal stresses on the line $x' = 0$, are given by the following relation

$$\tan 2\theta = \frac{(1-k)c^2 \cdot \left(\frac{b}{a}\right)^2 \sin 2\alpha}{(\cos^2\alpha + k\sin^2\alpha) - \left(\frac{b}{a}\right)^2(1 + \nu c^2 - c^2)(\sin^2\alpha + k\cos^2\alpha)}. \quad \text{(A35)}$$

Equation (A35) shows that θ tends to zero as b/a tends to zero. The values of θ for $b/a = 1/10$ and $k = 1/2$ are shown in Table A2, with α as 30, 60 and 80°. For a long narrow plate, θ always remains small unless α is close to 90°. If the stresses exceed the tensile strength an extension fracture should form at the middle of the plate approximately at a right angle to the plate length.

It may be noted that when $k = 0$, i.e. for a uniaxial extension in the plane of the plate, equation (A34) becomes the same as equation (A10), while for the symmetrical case, with $\alpha = 0$, the primed co-ordinates change to unprimed co-ordinates and equation (A34) becomes the same as equation (A29).